Cell type-specific expression of angiotensin receptors in the human lung with implications for health, aging, and chronic disease

Authors: Kynon JM Benjamin[1,2*], Maor Sauler[3], Hataya Poonyagariyagorn[4], and Enid R Neptune[4,5*]

[1]Lieber Institute for Brain Development, Baltimore, MD, USA
[2]Department of Neurology, Johns Hopkins University School of Medicine, Baltimore, MD, USA
[3]Pulmonary, Critical Care and Sleep Medicine, Yale School of Medicine, New Haven, CT, USA
[4]Division of Pulmonary and Critical Care Medicine, Johns Hopkins University School of Medicine, Baltimore, MD, USA
[5]Institute of Genetic Medicine, Johns Hopkins University School of Medicine, Baltimore, MD, USA

*Corresponding authors: Kynon JM Benjamin, KynonJade.Benjamin@libd.org; Enid Neptune, eneptune@jhmi.edu

Abstract

The renin-angiotensin system is a highly characterized integrative pathway in mammalian homeostasis whose clinical spectrum has been expanded to lung disorders such as chronic obstructive pulmonary disease (COPD)-emphysema, idiopathic pulmonary fibrosis (IPF), and COVID pathogenesis. Despite this widespread interest, specific localization of this receptor family in the mammalian lung is limited, partially due to the imprecision of available antibody reagents. In this study, we establish the expression pattern of the two predominant angiotensin receptors in the human lung, *AGTR1* and *AGTR2*, using complementary and comprehensive bulk and single-cell RNA-sequence datasets that are publicly available. We show these two receptors have distinct localization patterns and developmental trajectories in the human lung, pericytes for *AGTR1* and a subtype of alveolar epithelial type 2 cells for *AGTR2*. In the context of disease, we further pinpoint *AGTR2* localization to the COPD-associated subpopulation of alveolar epithelial type 2 ($AT2_B$) and *AGTR1* localization to fibroblasts, where their expression is upregulated in individuals with COPD, but not in individuals with IPF. Finally, we examine the genetic variation of the angiotensin receptors, finding *AGTR2* associated with lung phenotype (i.e., cystic fibrosis) via rs1403543. Together, our findings provide a critical foundation for delineating this pathway's role in lung homeostasis and constructing rational approaches for targeting specific lung disorders.

Main

The renin-angiotensin system (RAS), an extensively characterized hormonal network, plays a crucial role in maintaining the balance and stability of mammalian tissue functions. Dysregulated RAS contributes to numerous common disorders, such as hypertension, chronic renal disease, and heart failure[1], supporting the widespread use of RAS-targeting therapies. In fact, angiotensin receptor blockers (ARBs) and angiotensin-converting enzyme inhibitors are consistently among the top 10 most prescribed medications in the US[2–8]. Recent evidence afforded a reconception of this system focusing on tissue-specific activities and diverse physiological consequences. The availability of multiple agents targeting this pathway, coupled with the high expression of angiotensin peptides in the setting of inflammation and tissue repair, has broadened their therapeutic potential to encompass lung

disorders[9], such as acute lung injury[10,11], idiopathic pulmonary fibrosis (IPF)[12], pulmonary hypertension[13,14], and chronic obstructive pulmonary disease (COPD)-emphysema[15,16]. Since the SARS-CoV-2 receptor (ACE-2) is an angiotensin-processing enzyme, recent clinical studies have even examined the role of this pathway in COVID-19 pathogenesis[17,18]. A reliable delineation of the abundance and cell-specific expression pattern of the two predominant angiotensin receptors in the lung is needed to fully explore the mechanisms by which RAS targeting could address complex lung disorders.

Despite this widespread interest in the therapeutic potential for lung disorders, the specific localization of the angiotensin receptor family in the mammalian lung has been elusive. One reason for the lack of localization data is the general imprecision of the available antibody reagents which has been insufficiently appreciated within the research community[19–21]. Consequently, many well-constructed studies have been published with inaccurate expression data leading to flawed conceptual frameworks for therapeutic interventions. We and others have observed promising benefits in mouse models with some technical variation, including ARB-mediated attenuation of airspace enlargement in emphysema (genetic[22,23] and cigarette smoke-induced[24,25]) and improved histology in lung fibrotic disorders[26,27]. However, clinical and preclinical trials of ARBs have shown variable efficacy[8,28–30]. This inconsistency can be attributed to several factors beyond the anatomic and physiologic differences between mice and humans: dosing restrictions in clinical trials and indistinct concepts of lung cell-specific receptor behaviors, ultimately undermining the construction of trials for maximal efficacy.

In this study, we establish the expression pattern of the two predominant angiotensin receptors in the human lung, *AGTR1* and *AGTR2*, using complementary and comprehensive bulk and single-cell RNA-sequence datasets that are publicly available. We then examine the localization of these receptors in the COPD and IPF lung where compartmental phenotypes are well established. Finally, we conflate the genetic associations of angiotensin receptors with phenotype data. These findings represent the most comprehensive assessment of angiotensin receptor expression in the human lung leveraging publicly available transcriptomic datasets and disease-specific profiles. Our findings clarify the spectrum of angiotensin signaling in the lung and establish a foundation for selecting angiotensin-targeting reagents with compartmental considerations for various lung disorders.

Results

Angiotensin receptors show distinct localization patterns and cell type specifications in the human lung

To investigate lung cell types expressing angiotensin receptors, we leveraged the most comprehensive human lung single-cell dataset from version 2 of the Human Lung Cell Atlas (HLCA)[31]. The core HLCA study harmonized cell annotations for 584,944 cells from 14 datasets and 107 individuals, spanning all lung compartments and circulating blood[31]. Using this comprehensive dataset, we found that angiotensin receptors 1 (*AGTR1*) and 2 (*AGTR2*) positive cells represented a small fraction (1.64%) of the total cells examined. Of these receptor-positive cells, fewer than 0.1% co-expressed both *AGTR1* and *AGTR2* (**Figure 1A**).

We next examined the locations of *AGTR1* and *AGTR2* positive cells and found them in distinct compartments within the lung (**Figure 1B**). Specifically, we found *AGTR1*-positive cells primarily expressed in the stromal lung compartment (Fisher's exact test, FDR < 0.05; **Figure 1C**), with the highest expression observed in pericytes (48.2% of total cells; Fisher's exact test, FDR < 0.05; **Figure 1D** and **Figure S1**). Other stromal cell types, including vascular smooth muscle (6.4% of total cells), adventitial fibroblasts (14.7% of total cells), alveolar fibroblasts (13.2% of total cells), and peribronchial fibroblasts (4.0% of total cells), also showed significant enrichment for *AGTR1*-positive cells (Fisher's exact test, FDR < 0.05; **Figure 1D** and **Figure S1**). In contrast, we found *AGTR2*-positive cells primarily expressed in the lung epithelial compartment (**Figure 1C**), with the highest concentration in alveolar epithelial type 2 cells (AT2; 8.4% of total cells). Alveolar macrophages (0.048% of total cells) also showed enrichment of *AGTR2*-positive cells (Fisher's exact test, FDR < 0.05; **Figure 1D** and **Figure S1**). Interestingly, while both receptors represented a small proportion of overall lung cells, *AGTR1* dominated within pericyte cells, constituting nearly half of this cell population. Furthermore, we found that *AGTR1* and *AGTR2* each contributed roughly half of the total angiotensin receptor-positive cell population in this dataset. However, it is important to note that this dataset had relatively low proportions of stromal cells (25,217 [4.3%] cells) compared with epithelial (282,065 [48.2%] cells) and immune (229,496 [39.2%] cells). This suggests that *AGTR2*-positive cells are an extremely rare population compared to *AGTR1*-positive cells in the lung. Overall, these findings demonstrate a clear pattern of cell-specific and mutually exclusive expression for *AGTR1* and *AGTR2* across the human lung.

Limited information exists concerning angiotensin signaling in pericytes – a multipotent cell type residing in the vascular bed and known to be involved in vascular development and hemodynamic regulation. Since marker and ontogeny-defined subtypes of pericytes were recently described, we examined whether gene expression patterns in *AGTR1*-positive cells were associated with distinct classes or transitional states. We assessed subclusters of pericytes and projected the data using PHATE[32] (potential of heat-diffusion for affinity-based trajectory embedding) to preserve both local and global structures and capture potential transitions between cell states in pericytes. We found four distinct pericyte subclusters (**Figure 2A**). Although these four subclusters had various levels of *AGTR1* expression (**Figure 2B**), we did not find significant differences in *AGTR1* expression after correcting for patient variation (**Figure 2C**). These results suggest that *AGTR1* expression is a global marker gene for pericytes in the lung.

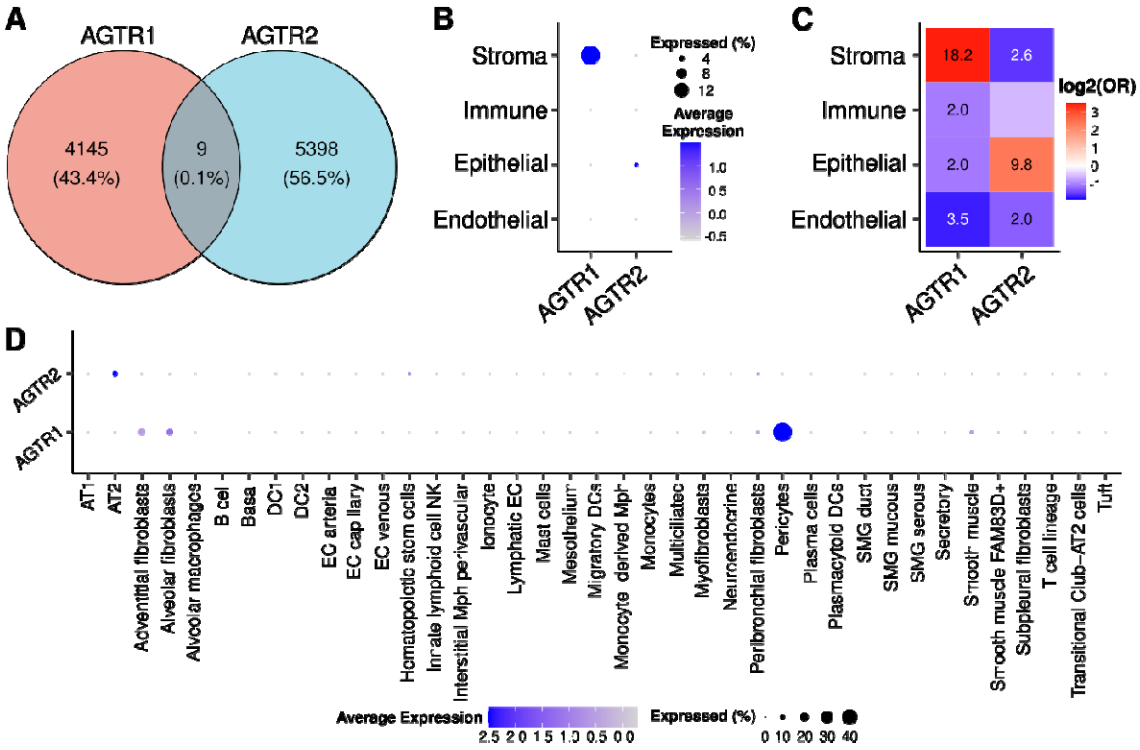

Figure 1: Angiotensin II receptors 1 (*AGTR1*) and 2 (*AGTR2*) demonstrate compartment- and cell-type-specific expression in the human lung. A. Venn diagram showing rare occurrences of *AGTR1* and *AGTR2* co-expression (n=107 individuals). **B.** Dot plot showing the percentage and average expression of *AGTR1*- and *AGTR2*-positive cells across lung compartments (n=107). **C.** Heatmap showing significant enrichment (two-sided, Fisher's exact test) of *AGTR1*- and *AGTR2*-positive cells across lung compartments (n=107). The color intensity of enrichment heatmaps represents log2 of odds ratio (OR) with red indicating enrichment and blue indicating depletion. Significantly enrichment compartments are annotated with -log10(false discovery rate). **D.** Dotplot showing the percentage and average expression of *AGTR1*- and *AGTR2*-positive cells across lung cell types (n=107).

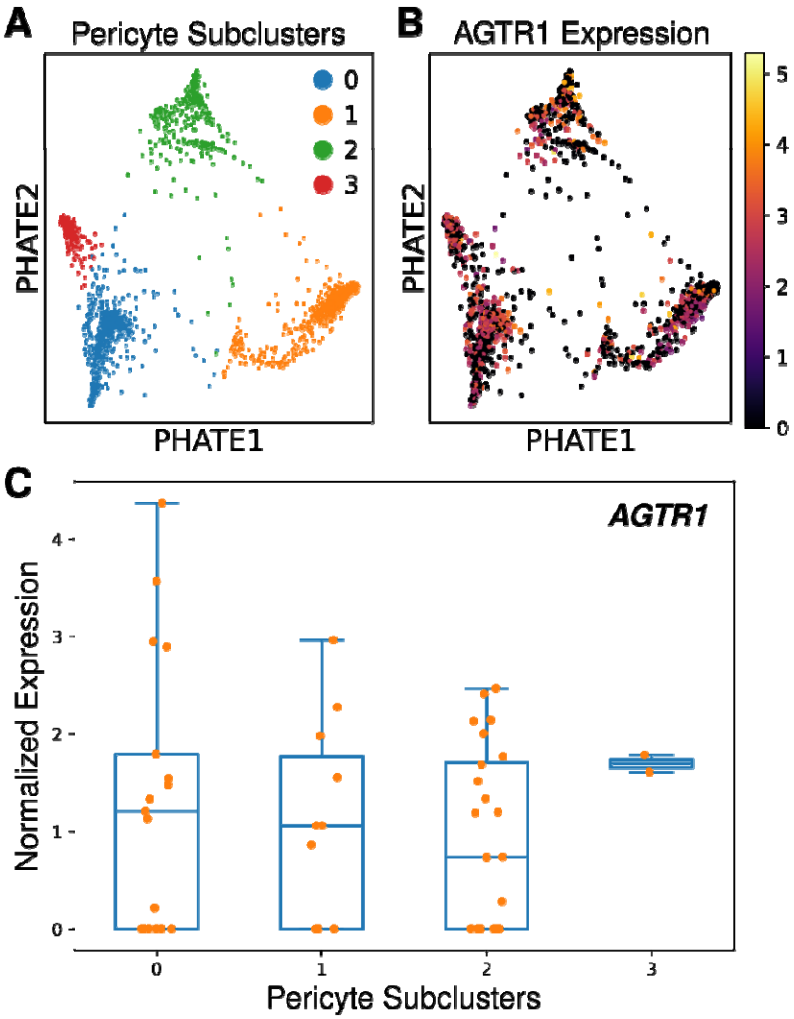

Figure 2: *AGTR1* is a global marker for pericytes. A. Scatter plot showing pericyte subclusters with PHATE dimensional reduction[32]. Subclusters are highlighted using K-means clustering. **B.** Scatter plot showing normalized expression of *AGTR1* across pericyte subclusters. **C.** Box plot showing no significant differences of *AGTR1* normalized expression across pericyte subclusters after averaging across individuals (n=107 across clusters). Box plots show the median and first and third quartiles, and whiskers extend to 1.5x the interquartile range.

Angiotensin receptors show distinct developmental trajectories in the human lung

After establishing distinct localization and expression patterns of the angiotensin receptors, we next asked how these receptors were expressed through postnatal development. To this end, we examined the ontogeny of angiotensin receptor expression from the neonatal period through young adulthood at the single-cell level using the integrated LungMAP dataset[33]. The type 1 receptor, *AGTR1,* showed the highest level of lung expression during infancy (31 weeks) with a steady reduction during childhood (3 years) and adulthood (31 years). In contrast, *AGTR2* displayed significantly lower levels of expression compared to *AGTR1*, which were maintained during the different stages of development (linear regression, FDR < 0.05; **Figure 3A**). The normalized expression of *AGTR1* in the mesenchymal stromal compartment was stable during infancy through adulthood suggesting that the overall

reduction in expression reflects a loss in the highest expressing cell types (pericytes and vascular smooth muscle cells; **Figure 3A** and **Figure S2A**). In contrast, the epithelial expression of *AGTR2* increased significantly in the adult lung compared with infancy and childhood (AT2; **Figure 3B** and **Figure S2B**). These trajectories correspond to distinct cell type-specific expression between the angiotensin receptors across development (**Figure S3**) and were replicated in cell-specific ontogeny bulk RNA-sequencing data from LungMAP (**Figure 4A** and **Figure S4**).

Given the increased prevalence of several lung disorders with age[34], and considering the relatively young donors in the LungMAP, we examined angiotensin receptor expression from mid- to late-life (age range = 21 to 70) using the GTEx v8 bulk lung RNA-sequencing data[35] (n=578; median age=56). Our analysis found a slight increase in *AGTR1* expression over time (Pearson, rho = 0.12, $p < 0.0052$; **Figure 4B**), while *AGTR2* expression decreased (Pearson, rho = -0.23, $p < 1.3e-8$; **Figure 4B**). Notably, *AGTR2* expression showed greater individual variation compared with *AGTR1*, potentially due to differences in cellular composition. To investigate this possibility, we performed cell deconvolution using BayesPrism[36] with the HLCA version 2 dataset as the single-cell reference (**Figure S5**). We found a negative correlation between age and AT2 cell type proportion but not alveolar macrophages (Pearson, rho = -0.35 and 0.0066, p-value < 2.2e-16 and p-value = 0.87 for AT2 and alveolar macrophage, respectively; **Figure 4C**). Moreover, AT2 cell type proportion directly correlated with *AGTR2* normalized expression (Pearson, rho = 0.78, p-value < 2.2e-16; **Figure 4C**). Conversely, the proportion of pericytes – the cell type most enriched for *AGTR1*-positive cells – showed a positive correlation with age (Pearson, rho = 0.17, p-value = 3.5e-5; **Figure 4D**). When we expanded this analysis to the other four *AGTR1* enriched cell types (i.e., adventitial fibroblasts, alveolar fibroblasts, peribronchial fibroblasts, and smooth muscle), we also found that adventitial fibroblasts and alveolar fibroblasts cell types showed a positive correlation with age (Pearson, rho = 0.095 and 0.23, p-value = 0.022 and 3.8e-8, respectively; **Figure 4D**). Furthermore, normalized *AGTR1* expression only increased with pericytes and alveolar fibroblasts cell type proportion (Pearson, rho = 0.35 and 0.25, p-value < 2.2e-16 and p-value = 7.7e-10, respectively; **Figure 4E**). These findings suggest that age-related upregulation of *AGTR1* expression is driven by changes in both pericyte and alveolar fibroblast populations.

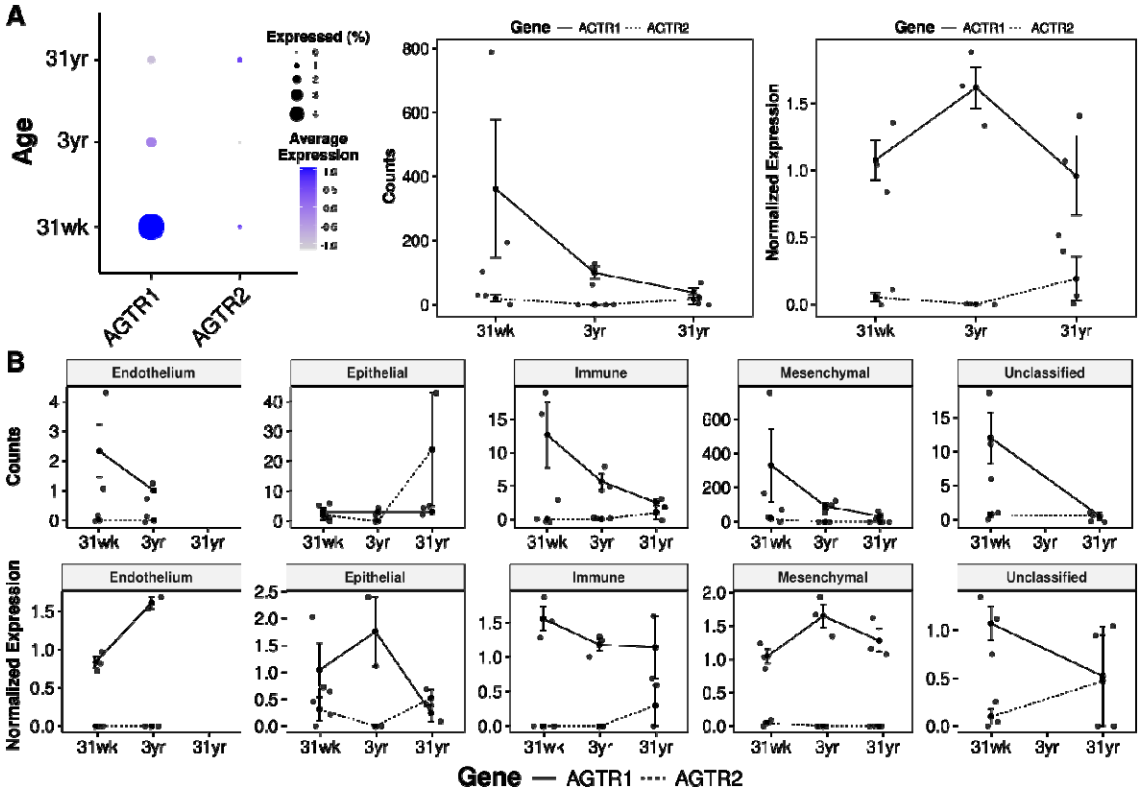

Figure 3: Angiotensin receptors, *AGTR1* and *AGTR2*, show distinct developmental trajectories across the lung location. A. Dotplot of average expression and percent expression from total cells separated by age. **B.** Line graph showing average number of cells (left) and log normalized expression (right) as a function of age. **C.** Line graph showing average number of cells (top) and log normalized expression (bottom) as a function of age separated by LungMAP annotated lung location. Three donors per age group. The standard error is annotated with error bars for all line graphs. Mean averaged across the three unique individuals are also annotated within the error bars, shown as standard error, of the line graphs. Solid line, *AGTR1*. Dash line, *AGTR2*.

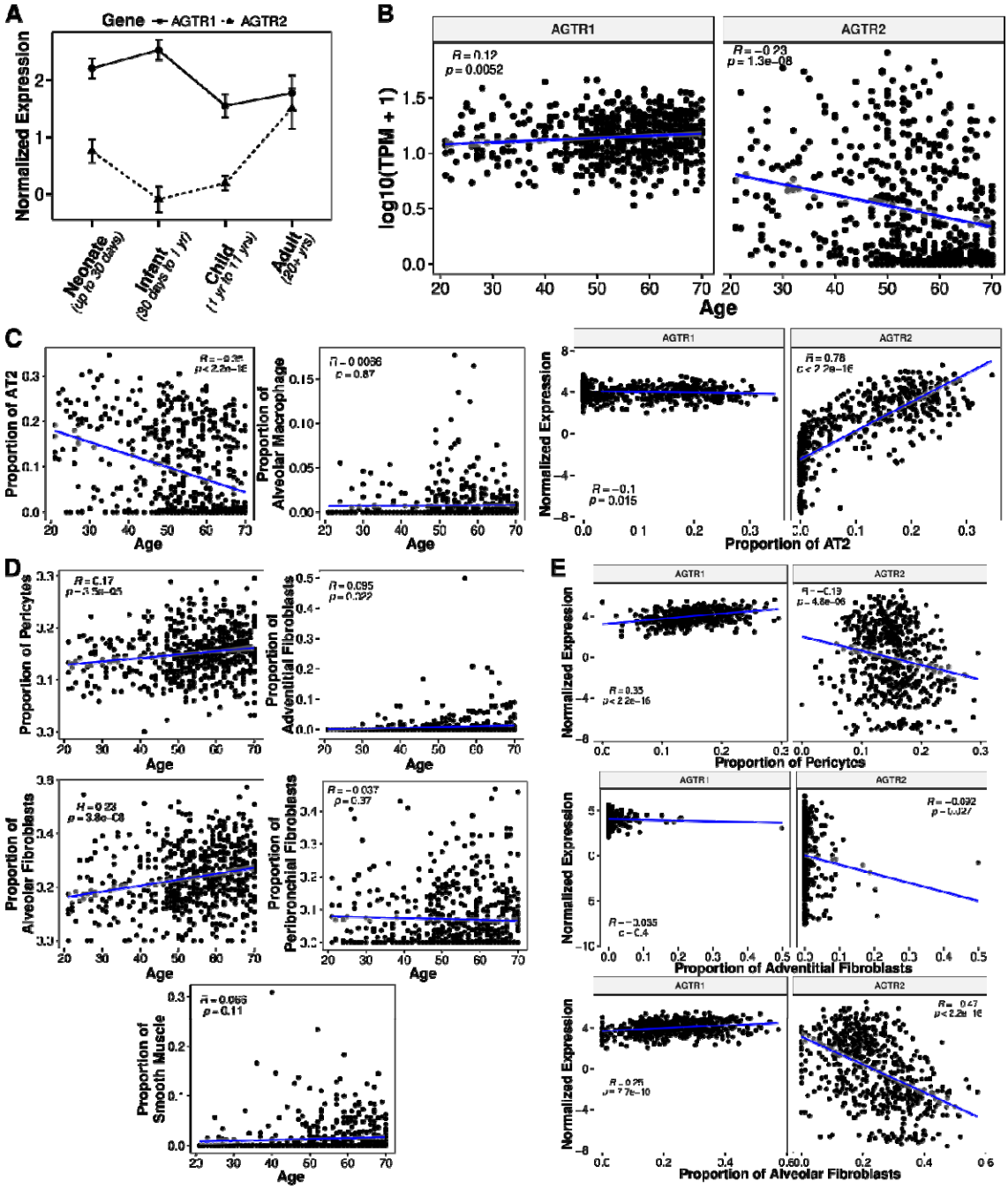

Figure 4: Replication of the angiotensin receptors' distinct developmental trajectories in bulk RNA-sequence analysis. A. Line graph of log2 normalized expression in bulk LungMAP lung tissue (n=3 per age group; error bars, standard error). Solid line, *AGTR1*. Dash line, *AGTR2*. **B.** Scatterplots of angiotensin receptors showing normalized expression as a function of age in adults (age > 20) from GTEx bulk lung tissue (n=578). **C.** Scatterplot showing the proportion of AT2 (alveolar epithelial type 2) and alveolar macrophage cell types from deconvoluted GTEx bulk tissue decreasing as a function of age (left), while normalized *AGTR2* expression increased with AT2 proportion (right). **D.** Scatterplot showing the cell type proportions of cell types enriched for *AGTR1* enriched cells (i.e., pericytes, adventitial fibroblasts, alveolar fibroblasts, peribronchial fibroblasts, and smooth muscle) from deconvoluted GTEx bulk tissue as a function of age. **E.** Scatterplots of normalized

angiotensin receptors expression as a function of pericytes (top), adventitial fibroblasts (middle), and alveolar fibroblasts (bottom) cell type proportions. Blue line fitted trend (two-sided, Pearson's correlation). The 95% confidence interval is shaded in gray.

Angiotensin receptor dynamics in individuals with COPD and IPF

Although multiple observational and preclinical studies suggest that ARBs may confer some functional and/or histologic benefit in COPD and IPF, the receptor expression patterns in the lung associated with the disease states have not been elucidated. Since the angiotensin II peptide can interact with both angiotensin receptors, blockade of the AT1R could plausibly increase peptide engagement with the AT2R, creating alternative mechanisms of possible efficacy[37]. We next explored the expression pattern of angiotensin receptors in COPD and IPF. To this end, we re-examined a human lung COPD and IPF single-cell dataset (IPF [n=32], COPD [n=18], and control donor lungs [n=28][38]). Consistent with our prior observations, we found little overlap between *AGTR1* and *AGTR2* positive cells (**Figure 5A**), and distinct localization within the lung (**Figure S6**). Furthermore, *AGTR2*-positive cells appeared more prevalent in COPD, while *AGTR1*-positive cells were associated with IPF (**Figure 5B**). We also observed a significant upregulation of *AGTR1* in fibroblast cells of COPD patients (t-test, $p < 0.013$; **Figure 5C**). Although the average *AGTR1* expression was highest in IPF patients, we did not identify a specific cell type with a significantly different normalized expression between IPF patients and controls for either receptor (**Figure 5C** and **Figure S7**). However, the proportion of individuals with *AGTR1*-positive cells was higher in IPF patients (94%) compared to control donors (75%) or COPD patients (78%), potentially explaining the observed discrepancy.

While we did not observe a statistically significant upregulation of *AGTR2* in AT2 cells by disease state, there was a trend towards increased expression in COPD patients (t-test, p-value = 0.14; **Figure 5D**). A previous study identified specific COPD-associated cell types within a subpopulation of AT2 cells[39], prompting us to re-examine this dataset for *AGTR2* dysregulation for COPD (COPD [n=17] and age-matched control lungs [n=15][39]). We found that *AGTR2* expression was primarily associated with the $AT2_B$ subpopulation of AT2 cells (expressed in 8.4% of $AT2_B$ cells; **Figure 5F**), which is the specific COPD-contributing cell type previously reported[39]. Within this $AT2_B$ cell type, *AGTR2* expression significantly increased in COPD patients compared with age-matched controls (t-test, p-value < 0.033; **Figure 5E**). Additionally, when we assessed subclusters of AT2 cells in the IPF/COPD dataset with PHATE[32] (**Figure 5G**), we also found a significant increase in *AGTR2* expression in a specific subcluster of AT2 cells in COPD (t-test, p-value < 0.0036; **Figure 5H**). Moreover, we replicated this increase in *Agtr2* expression using a cigarette smoke mouse model (t-test, p-value < 0.00012; **Figure S8**).

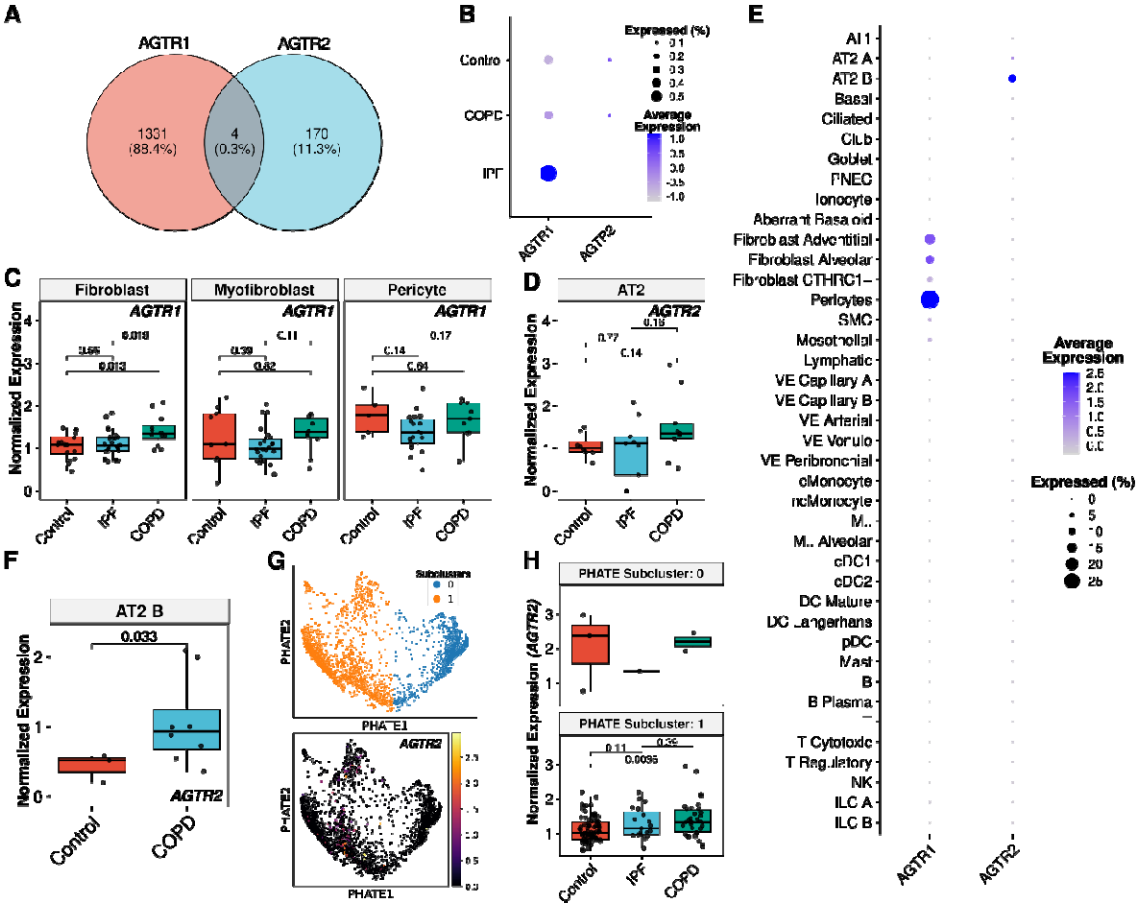

Figure 5: Fibroblasts and alveolar epithelial type 2 (AT2 subpopulation) are significantly upregulated in individuals with COPD for *AGTR1* and *AGTR2*, respectively. A. Venn diagram showing limited co-occurrence of *AGTR1* and *AGTR2* expression in the same cell (control [n=28], COPD [n=18], or IPF [n=32][38]). **B.** Dotplot of average and percent expression of angiotensin receptors from total cells separated by diagnosis (control [n=28], COPD [n=18], or IPF [n=32][38]). Box plot comparing IPF (n=32), COPD (n=18), and control donors (n=28) normalized expression for cell types enriched for **C.** *AGTR1*-positive cells and **D.** *AGTR2*-positive cells. **E.** Dotplot of average and percent expression of angiotensin receptors showing enrichment of *AGTR2* expression for AT2 subpopulation ($AT2_B$; COPD [n=17] and age-matched control donors [n=15][39]). **F.** Box plot of normalized expression for AT2 subpopulation ($AT2_B$) comparing COPD (n=17) and age-matched control donors (n=15). **G.** Replication of *AGTR2* upregulation for COPD for AT2 subpopulation within IPF/COPD dataset (control [n=28], COPD [n=18], or IPF [n=32][38]). Top: Dimensional reduction using PHATE[32] of AT2 in IPF/COPD dataset showing two subclusters (0 and 1). Bottom: Heatmap showing limited expression of *AGTR2* specific to PHATE subcluster 1. **H.** Box plot of normalized expression for PHATE AT2 subclusters showing increased expression of *AGTR2* for COPD compared with control donors. Box plots are annotated with a two-sided, t-test and show the median and first and third quartiles, and whiskers extend to 1.5x the interquartile range.

Genetic variation of angiotensin receptors in the human lung

Recently described common genetic variants in angiotensin receptors plausibly contribute to cardiovascular and renal disorders, particularly those related to systemic hypertension[40–42]. We first identified angiotensin expression quantitative trait loci (eQTL) in the human lung to understand genetic variation associated with angiotensin receptors and lung disease. To this end, we re-processed GTEx lung data (n=578) and found 198 and 179 cis-eQTL (permutation q-value < 0.05; **Table S1**) for *AGTR1* and *AGTR2*, respectively. Of these cis-eQTL, we found three variants with conditionally independent signals (nominal p-value < 5.6e-5; **Table S2**) for *AGTR1* (rs4681418, rs12487698, and rs11371912) and *AGTR2* (rs1403543, rs1589657, and rs6608481).

Following conditional analysis, we performed fine mapping using the Sum of Single Effects (SuSiE;[43]) and identified three credible SNP (single nucleotide polymorphism) sets for each gene (**Table S3**). We found these credible SNPs replicated using other fine-mapping approaches (**Table S4-S7**;[44–46]). For *AGTR1*, we found the three conditional variants (rs4681418, rs12487698, and rs11371912) showed the highest posterior inclusion probability (PIP) within each credible SNP set. For *AGTR2*, we found two of the three (rs1403543 and rs6608481) showed the highest PIP, and a third variant (rs5991094) showed a higher PIP compared to the conditionally independent signal (rs1589657) for their respective credible SNP sets.

We next examined these SNPs for PheWAS associations using the genome-wide association studies (GWAS) Catalog of SNPs[47]. While there were no associations with *AGTR1*, we found 50 phenotypes significantly associated (p-value < 0.05; **Table S8**) with *AGTR2*, all attributed to variant rs1403543. Interestingly, this variant also showed an association with cystic fibrosis severity GWAS (p-value = 2e-6;[48]). No other fine-mapped variant has been previously reported to be associated with any phenotype. This is primarily due to the lack of a significant eQTL for rs5186 (nominal p-value = 0.092) – clinically linked with genetic variants regulating *AGTR1* and hypertension GTEx lung[40–42] – in the GTEx lung data.

Discussion

The RAS system, including the angiotensin receptors, has been associated with common disorders and is currently targeted for therapeutic intervention for lung disorders like COPD and IPF. Even so, the specific localization of this receptor family in the mammalian lung is poorly understood. Here, we leverage publicly available datasets to systematically examine the two predominant angiotensin receptors, *AGTR1* and *AGTR2*, in the human lung at cellular resolution. We find distinct receptor expression patterns in the lung with postnatal development, aging, and lung diseases such as COPD and IPF, supporting a plausible role of angiotensin signaling in defined disease states. Furthermore, our fine-mapping results identified a genetic variant (rs1403543) associated with *AGTR2* and cystic fibrosis severity. Altogether, this provides a detailed summary of angiotensin II receptor expression across the human lung and the relevance of this expression profile to the COPD and IPF disease states.

Across multiple single-cell datasets, we analyzed angiotensin receptor expression in different human lung compartments (endothelial, epithelial, mesenchymal [stromal], and

immune) and cell types. While angiotensin receptor-positive cells represent a minority of the total lung cell population, they notably constitute roughly 25% of all stromal cells (both vascular and alveolar). We further show that *AGTR1* and *AGTR2* have mutually exclusive expression and distinct localization within the lung. *AGTR1* is primarily expressed in the stromal compartment, particularly pericytes, where around half of all pericytes express this receptor. In contrast, *AGTR2* is primarily located in the lung epithelium, specifically within an AT2 subpopulation previously defined as $AT2_B$, where only 8.4% of the cells express it. AT2 cells play important roles in normal pulmonary function and the lung response to toxic compounds[49]. Other studies have shown the involvement of lung pericytes in the development of various lung diseases including asthma, pulmonary fibrosis, pulmonary hypertension, and sepsis[50,51]. Altogether, these specific cell type localizations suggest the potential contributions of these angiotensin receptors to the pathogenesis of these lung diseases.

The finding that roughly half of all lung pericytes expressed *AGTR1* is especially notable. Our inability to identify a distinct *AGTR1*-positive pericyte subtype suggests that AGTR1 expression might be ubiquitous across all pericytes. This observation could potentially be attributed to technical limitations of single-cell analysis, such as dropout events.

Our survey showed *AGTR2* expression in alveolar epithelial cells. The low abundance of *AGTR2*-expressing cells in the lung invokes the possibility that these cells mark a subtype with specific localization and specific function. Indeed, we found upregulation of *AGTR2* in COPD patients associated with a subtype of AT2 cells. The expansion of *AGTR2*-expressing cells in COPD lungs and *Agtr2* expression in mouse lungs exposed to chronic cigarette smoke creates a hypothetical rationale for therapeutic targeting of this receptor for these disorders. We recently showed that *Agtr2* activation attenuates hyperoxic acute lung injury in adult mice[37]. In that study, we found that *Agtr2* agonists reduce oxidative stress and TGF-β activation, two injury measures also associated with chronic cigarette smoke-induced lung injury[24]. Ongoing clinical trials of AGTR2 activators for IPF may further demonstrate valid clinical and biological metrics that could be extended to COPD trials[52].

We observed negligible angiotensin receptor expression in immune and endothelial cell types. This aligns with previous findings that angiotensin II's inflammatory effects are mediated by mesenchymal cells. These cells are thought to recruit inflammatory cells and activate the NLRP3 inflammasome in an autocrine manner[53], leading to a paracrine inflammatory response. This evidence suggests that angiotensin receptor-positive stromal cells, including pericytes, may act as immune regulators in the lung. The prominent expression of *AGTR1* in pericytes, which is closely associated with endothelial cells in the microvasculature, presents a compelling opportunity for further investigation. Definitive studies establishing this relationship could reflect a new paradigm for vascular dysfunction, potentially leading to therapeutic strategies involving angiotensin receptor blockade. Additionally, future studies could explore the possibility that angiotensin receptor expression in immune and endothelial cells might be induced under specific conditions of tissue injury.

The cell type distribution of the receptors showed distinctive patterns over time. We found stromal *AGTR1* expression stable during infancy through adulthood. When we examined mid- to late-life (age > 30) with deconvoluted bulk lung expression, we found a significant slight increase of *AGTR1* expression specific to alveolar fibroblast cells. Interestingly, we found upregulation of *AGTR1* in COPD patients associated with the fibroblast population,

consistent with the designation of COPD as a disorder of accelerated aging[54]. On the other hand, *AGTR2* expression increases significantly in adult lungs compared with infancy (31 weeks) or childhood (3 years). Furthermore, *AGTR2* expression in AT2 cells decreased with age in sharp contrast to an increase in expression in COPD patients compared to age-matched controls. Although our study did not identify a direct link between angiotensin receptor expression with IPF, the findings suggest a potential role for angiotensin receptors in COPD. First, *AGTR1* expression in fibroblasts might serve as a biomarker for COPD and potentially confer a productive signaling axis. Second, the upregulation of *AGTR2* in a subset of AT2 cells in COPD patients and mice exposed to chronic cigarette smoke might represent a marker for the cell injury state or, as considered above, a signaling portal for modulation.

In addition to exploring the expression of *AGTR1* and *AGTR2*, we examined genetic variation in the human lung using the GTEx dataset. The three fine-mapped variants (rs4681418, rs12487698, and rs11371912) associated with *AGTR1* were not associated with any phenotype from the PheWAS catalog. Interestingly, we did not identify an *AGTR1* eQTL for rs5186 – clinically associated with hypertension[40–42] – in the postmortem lung. Additionally, this variant was only identified for *CPA3* (mast cell carboxypeptidase A3) in sun-exposed skin and the esophagus mucosa in the GTEx dataset. Although the GTEx dataset has limited diversity, the lack of observed eQTL for the *AGTR1*-rs5186 gene-SNP pair was surprising.

For *AGTR2*, we found one of the three fine-mapped variants, rs1403543, had been previously associated with cystic fibrosis severity[48]. While we did not find an association with COPD or IPF in the PheWAS catalog, we suspect this is primarily due to the exclusion of the X-chromosome where *AGTR2* is located from the majority of GWAS[55], including COPD GWAS. Renewed efforts to include the X chromosome have resulted in a new X chromosome-wide association study for COPD[56]. While this XWAS and meta-analysis of COPD datasets did not identify any of the *AGTR2* fine-mapped SNPs, they highlight the heritability of the X chromosome for COPD and allow for future colocalization analyses.

Transcriptomic data analysis relies heavily on the quality of the starting genetic material. The clinical cohorts that we interrogated varied in size and depth of analyses. However, the consistency observed in angiotensin receptor expression patterns across these diverse datasets (HLCA, GTEx, and LungMap) strengthens our findings. Nonetheless, further validation in larger cohorts with greater inclusion of lung disease subtypes is needed to confirm the specific cell populations expressing these receptors in different disease contexts.

In summary, we integrate multiple publicly available datasets to reveal the cell-specific and compartmental localization of the major angiotensin receptors (*AGTR1* and *AGTR2*) in the human lung. We further explored how these patterns vary with age and chronic lung disease status. Our findings establish the *AGTR1* as a reliable and highly selective marker of lung pericytes with functional relevance in the airspace compartment where ARBs have shown promise in preclinical models. Similarly, the detection of *AGTR2* expression in a subset of the alveolar epithelial compartment coupled with increased levels in COPD, invites consideration of its role as a therapeutic target. Overall, our analysis using publicly available data provides a nimble foundation for exploring the targeted use of available drugs to treat chronic and debilitating lung disorders. Furthermore, our strategy demonstrates the potential

of large transcriptomic datasets to refine our understanding of other receptors lacking other reliable detection methods.

Methods

Ethical statement

This study used publicly available datasets where informed consent procedures were established for each study as described in the original papers[31,33,35,38,39]. Specifically, the Human Lung Cell Atlas[31] involved a multi-study integrative analysis, with each study documenting informed consent as referenced in the original studies. The LungMAP[33] dataset involved donor lung procurement following protocols approved by the Institutional Review Board (IRB) at the University of Rochester Medical Center (RSRB00047606). For the GTEx dataset[35], deceased donor tissues were obtained through next-of-kin consent for scientific research, following procedures established by the Biospecimen Source Sites (BSS) and overseen by the relevant Institutional Review Boards (IRBs) or deemed exempt from IRB review due to the deceased status of the donors. The COPD/IPF studies[38,39] involving human samples adhered to informed consent protocols and data publication guidelines approved by the Partners Healthcare Institutional Review Board (IRB Protocol 2011P002419).

Human lung data download

We downloaded HDF5 files for the Human Lung Cell Atlas[31] from CellxGene at https://cellxgene.cziscience.com/collections/6f6d381a-7701-4781-935c-db10d30de293. We downloaded counts and metadata for single-cell and bulk LungMap[33] data from the LungMap website (c). We downloaded GTEx v8[35] whole genome sequencing VCF, bulk RNA-sequencing, phenotype information, and cis-eQTL GTEx covariates including the PEER (probabilistic estimation of expression residuals) factors[57] from the GTEx portal (https://gtexportal.org/home/datasets). We downloaded raw counts, cell type annotations, and metadata for IPF and COPD single-cell RNA sequencing data[38,39] (GEO; GSE136831).

Human lung dataset population characteristics

The single-cell lung datasets encompass diverse population characteristics. The HLCA Core dataset includes samples from 107 individuals with diversity in age, sex, and self-identified socially relevant group, with 65% European, 14% African, 2% Admixed American, 2% multi-ancestry, 2% Asian, 0.4% Pacific Islander, and 14% unannotated ancestry, harmonized to 1000 genomes reference superpopulations. This dataset includes 40% female participants. The LungMap dataset for single-cell analysis consists of individuals of European ancestry, with samples from 2 males and 1 female at 31 weeks, 2 males and 1 female at 3 years, and 1 male and 2 females at 31 years. The IPF/COPD single-cell dataset included 78 individuals, with 73 self-reported as white, 1 Black, 1 Latino, 2 Asian, and 1 other. The sex distribution was 35% female (27 females, 51 males), and the age range was 20 to 80 years (median 62 years, mean 57.6 ± 14.47). Additionally, 56% reported ever smoking.

Regarding the bulk lung datasets, the LungMap dataset included self-reported races of 6 Black, 2 other, 5 unknown, and 13 white individuals. The donor sex distribution was 8 females and 18 males, with an age range from neonates to 40 years, including 4 neonates, 9 infants, 11 children, and 2 adults, with at least one female or male represented in each age cohort. The GTEx bulk lung dataset comprised 578 individuals aged 21 to 70 years (median

56, mean 53.97 ± 11.84), with 183 females and 395 males. The self-reported/study-reported race distribution was 493 white, 70 Black, 10 Asian, 1 other, and 4 unknown individuals.

Mice

We obtained adult AKR/J mice from the Jackson Laboratory. These mice were housed in a facility accredited by the American Association of Laboratory Animal Care. The Johns Hopkins University School of Medicine's Institutional Animal Care and Use Committee reviewed and approved the animal studies.

Cigarette smoke exposure

We divided six- to eight-week-old AKR/J male mice into two groups. We placed the control group in a filtered air environment. The experimental group received cigarette smoke exposure mixed with drinking water for six to seven weeks. This exposure involved burning 2R4F reference cigarettes (University of Kentucky, Louisville, Kentucky, USA) for two hours per day, five days a week, using a smoking machine (Model TE-10; Teague Enterprises). We routinely monitored the average concentration of total suspended particulates and carbon monoxide, maintained at 90 mg/m and 350 ppm, respectively.

Angiotensin receptor single-cell expression profiling

Normalization and quality control

For angiotensin receptor single-cell expression profiling, we first normalized counts using `scuttle` (version 1.12.0;[58]) *logNormCounts* on `SingleCellExperiment` (version 1.24.0;[59]) objects in R (version 4.3). Following normalization, we computed the sum factors before adding per cell and feature quality control (QC) information with `scuttle`. After initial QC annotation, we performed quality control based on the dataset. Specifically, for HLCA version 2, we found the provided data had very limited mitochondria percentage. Therefore, we did not filter specifically for mitochondria percentage. Instead, we removed outliers based on `scuttle` *perCellQCFilters*. For LungMap 10x, we removed cells with greater than 25% mitochondria-mapped reads and library size less than 1000. For the IPF/COPD dataset, we removed cells with greater than 25% mitochondria mapped reads and library sizes less than 1000. For the COPD replication dataset, we removed cells with greater than 20% mitochondria mapped reads and library size less than 1000 as previously described[39]. The remaining cells were used for angiotensin receptor expression profiling.

Statistical analysis

We performed a two-tailed Fisher's exact test to examine angiotensin receptor significant enrichment for cell annotations (compartment and cell annotation). Within each cell annotation, we performed multiple testing corrections using FDR. For developmental trajectories of the angiotensin receptors, we fitted a linear model on average expression by donor patient (n=3) separately for angiotensin receptor and cell annotation.

Cell-type subcluster analysis

For pericyte subcluster analysis, we subsetted HLCA version 2 for the pericyte cell type. For AT2 subclustering, we subsetted the IPF/COPD dataset for the AT2 cell type. In Python (version 3.9.16), we applied general filtering and quality control similar to the R version with `scprep` (version 1.2.3). Following quality control, we normalized library size and transformed counts with `scprep`. For dimensional reduction, we used `PHATE` (version 1.0.11;[32]) and estimated the *K* clusters visually with KDE plots (`seaborn`, version 0.13.2;[60]). *De novo* cluster annotation used the K-means algorithm from `PHATE`.
For pericyte subclusters, we compared *AGTR1* expression using two-sided, one-way ANOVA. For AT2 two cluster comparison, we compared *AGTR2* expression using a two-sided, T-test and a one-sided, Mann-Whitney U test.

Bulk RNA-sequencing age correlation

For GTEx analysis of angiotensin receptors in the human lung, we applied a linear model on $\log_{10}$ transformed TPM (transcripts per million) normalized expression as a function of age. We corrected for multiple testing with Bonferroni. For LungMap analysis of angiotensin receptors in the human lung, we applied a linear model on $\log_{10}$ transformed normalized expression as a function of age, adjusting for derivative type, donor sex, and donor self-identified race.

Cell-type deconvolution

We performed cell-type deconvolution using `BayesPrism` (version 2.2.2;[36]) in R (version 4.3) for GTEx lung and Human Lung Cell Atlas version 2 single-cell reference. Specifically, we selected cell type marker genes using *get_mean_ratio2* from `DeconvoBuddies` (developmental version) – selecting genes with a rank ratio less than or equal to 100 shared between the GTEx lung data and HLCA reference data. For the single-cell reference data, we removed ribosomal genes, mitochondria genes, *MATAL1*, and genes on the sex chromosomes following `BayesPrism` recommendations. We used the *new.prism* function with an outlier cutoff of 1% and an outlier fraction of 10%.

Real-time PCR (qPCR) analysis

We isolated total RNA from whole lung mouse tissues and treated it with DNase. Next, we reverse-transcribed the RNA using Invitrogen's first-strand DNA synthesis kit. The resulting cDNA was used for PCR analysis on an ABI Fast 7500 System (Applied Biosystems, Foster City, CA). Custom TaqMan probes for the genes of interest were designed by Applied Biosystems based on the sequences in the Illumina array and used according to the manufacturer's instructions. Expression levels of target genes were determined in triplicate from the standard curve and normalized to *Gapdh* mRNA.

Expression quantitative trait loci (eQTL) analysis

For bulk lung cis-eQTL analysis, we re-processed the GTEx data using `tensorQTL`[61] (version 1.0.8) as previously described[62,63] with modifications for lung tissue. Briefly, we filtered out low expression genes (< 0.1 TPM in at least 20% of samples) and normalized

counts using TMM (trimmed mean of M values). Following normalization, we performed cis-eQTL analysis using linear regression and GPU adjusting for genetic similarity (i.e., genotyping principal components) and PEER factors with a mapping window of 1 Mb of the TSS (transcriptional start site) for each gene and a minor allele frequency ≥ 0.05. We used PEER factors to adjust for hidden variation. We determined permutation q-values for the most highly associated variant per gene using empirical p-values based on default values in `tensorQTL`. Following permutation analysis, we performed conditional cis-eQTL analysis using the same parameters as the initial cis-eQTL analysis with tensorQTL.

Fine-mapping analysis

We performed fine mapping using `SuSiE`[43] implemented in Python with `tensorQTL`. We downloaded GTEx lung fine-mapping results with `CAVIAR`[44], `CaVEMaN`[45], and `DAP-G`[46] from the GTEx portal for replication.

Graphics

All plots were generated in R (version 4.3) or Python (version 3.9). For Venn diagrams comparing the overlap between *AGTR1* and *AGTR2*, we used `ggvenn` (version 0.1.10;[64]) in R. Dot plots showing average expression and percentage of positive expression angiotensin receptor cells were generated using the `Seurat` (version 5.0.1;[65]) *DotPlot* function in R. Line graphs, scatter plots, box plots, and bar plots were generated using `ggpubr` (version 0.6.0;[66]) in R. Heatmap enrichment plots were generated in R using `ggplot2` (version 3.5.0;[67]), `ggfittext` (version 0.10.2;), and `ggpubr`. PHATE subcluster plots visualization used the `scprep` *scatter2d* function and the subcluster box plot graphic was generated with `seaborn` in Python.

Data availability

The Human Lung Cell Atlas is a publicly available resource located at https://hlca.ds.czbiohub.org/. We downloaded HDF5 and RDS files associated with the HLCA version from CellxGene (https://cellxgene.cziscience.com/collections/6f6d381a-7701-4781-935c-db10d30de293). The LungMAP is a publicly available resource located at https://lungmap.net/. We downloaded data from Wang *et al.*[33] at https://data-browser.lungmap.net/explore/projects/20037472-ea1d-4ddb-9cd3-56a11a6f0f76. For COPD and IPF data, we downloaded raw counts and metadata from GEO (GSE136831)[38,39].

Code availability

All code, jupyter-notebooks, and results are available through GitHub at https://github.com/heart-gen/angiotensinII_lung.

References

1. Patel, S., Rauf, A., Khan, H. & Abu-Izneid, T. Renin-angiotensin-aldosterone (RAAS): The ubiquitous system for homeostasis and pathologies. *Biomed. Pharmacother. Biomedecine Pharmacother.* **94**, 317–325 (2017).
2. Kochanek, K., Murphy, S. L., Xu, J. & Arias, E. *Mortality in the United States, 2022*. https://stacks.cdc.gov/view/cdc/135850 (2023) doi:10.15620/cdc:135850.
3. Kuber, B., Fadnavis, M. & Chatterjee, B. Role of angiotensin receptor blockers in the context of Alzheimer's disease. *Fundam. Clin. Pharmacol.* **37**, 429–445 (2023).
4. Nakamura, K., Okuyama, R. & Kawakami, Y. Renin-Angiotensin System in the Tumor Microenvironment. *Adv. Exp. Med. Biol.* **1277**, 105–114 (2020).
5. Puskarich, M. A. *et al.* Efficacy of Losartan in Hospitalized Patients With COVID-19-Induced Lung Injury: A Randomized Clinical Trial. *JAMA Netw. Open* **5**, e222735 (2022).
6. Akioyamen, L. *et al.* Cardiovascular and cerebrovascular outcomes of long-term angiotensin receptor blockade: meta-analyses of trials in essential hypertension. *J. Am. Soc. Hypertens. JASH* **10**, 55-69.e1 (2016).
7. Bilen, Y. *et al.* Treatment and practical considerations of diabetic kidney disease. *Front. Med.* **10**, 1264497 (2023).
8. Wise, R. A. *et al.* Clinical Trial of Losartan for Pulmonary Emphysema: Pulmonary Trials Cooperative Losartan Effects on Emphysema Progression Clinical Trial. *Am. J. Respir. Crit. Care Med.* **206**, 838–845 (2022).
9. Suzuki, Y. *et al.* Inflammation and angiotensin II. *Int. J. Biochem. Cell Biol.* **35**, 881–900 (2003).
10. Marshall, R. P. *et al.* Angiotensin II and the fibroproliferative response to acute lung injury. *Am. J. Physiol. Lung Cell. Mol. Physiol.* **286**, L156-164 (2004).
11. Jerng, J.-S. *et al.* Role of the renin-angiotensin system in ventilator-induced lung injury: an in vivo study in a rat model. *Thorax* **62**, 527–535 (2007).

12. Otsuka, M., Takahashi, H., Shiratori, M., Chiba, H. & Abe, S. Reduction of bleomycin induced lung fibrosis by candesartan cilexetil, an angiotensin II type 1 receptor antagonist. *Thorax* **59**, 31–38 (2004).
13. Chassagne, C. *et al.* Modulation of angiotensin II receptor expression during development and regression of hypoxic pulmonary hypertension. *Am. J. Respir. Cell Mol. Biol.* **22**, 323–332 (2000).
14. Morrell, N. W., Morris, K. G. & Stenmark, K. R. Role of angiotensin-converting enzyme and angiotensin II in development of hypoxic pulmonary hypertension. *Am. J. Physiol.* **269**, H1186-1194 (1995).
15. Andreas, S. *et al.* Angiotensin II blockers in obstructive pulmonary disease: a randomised controlled trial. *Eur. Respir. J.* **27**, 972–979 (2006).
16. Shrikrishna, D., Astin, R., Kemp, P. R. & Hopkinson, N. S. Renin-angiotensin system blockade: a novel therapeutic approach in chronic obstructive pulmonary disease. *Clin. Sci. Lond. Engl. 1979* **123**, 487–498 (2012).
17. Mancia, G., Rea, F., Ludergnani, M., Apolone, G. & Corrao, G. Renin-Angiotensin-Aldosterone System Blockers and the Risk of Covid-19. *N. Engl. J. Med.* **382**, 2431–2440 (2020).
18. Fosbøl, E. L. *et al.* Association of Angiotensin-Converting Enzyme Inhibitor or Angiotensin Receptor Blocker Use With COVID-19 Diagnosis and Mortality. *JAMA* **324**, 168–177 (2020).
19. Benicky, J., Hafko, R., Sanchez-Lemus, E., Aguilera, G. & Saavedra, J. M. Six commercially available angiotensin II AT1 receptor antibodies are non-specific. *Cell. Mol. Neurobiol.* **32**, 1353–1365 (2012).
20. Herrera, M., Sparks, M. A., Alfonso-Pecchio, A. R., Harrison-Bernard, L. M. & Coffman, T. M. Lack of specificity of commercial antibodies leads to misidentification of angiotensin type 1 receptor protein. *Hypertens. Dallas Tex 1979* **61**, 253–258 (2013).
21. Hafko, R. *et al.* Commercially available angiotensin II At□ receptor antibodies are nonspecific. *PloS One* **8**, e69234 (2013).

22. Habashi, J. P. *et al.* Losartan, an AT1 antagonist, prevents aortic aneurysm in a mouse model of Marfan syndrome. *Science* **312**, 117–121 (2006).
23. Lee, J.-J., Galatioto, J., Rao, S., Ramirez, F. & Costa, K. D. Losartan Attenuates Degradation of Aorta and Lung Tissue Micromechanics in a Mouse Model of Severe Marfan Syndrome. *Ann. Biomed. Eng.* **44**, 2994–3006 (2016).
24. Podowski, M. *et al.* Angiotensin receptor blockade attenuates cigarette smoke-induced lung injury and rescues lung architecture in mice. *J. Clin. Invest.* **122**, 229–240 (2012).
25. Mei, D. *et al.* Angiotensin II type-2 receptor activation in alveolar macrophages mediates protection against cigarette smoke-induced chronic obstructive pulmonary disease. *Pharmacol. Res.* **184**, 106469 (2022).
26. Yao, H. W., Zhu, J. P., Zhao, M. H. & Lu, Y. Losartan attenuates bleomycin-induced pulmonary fibrosis in rats. *Respir. Int. Rev. Thorac. Dis.* **73**, 236–242 (2006).
27. Li, X., Rayford, H. & Uhal, B. D. Essential roles for angiotensin receptor AT1a in bleomycin-induced apoptosis and lung fibrosis in mice. *Am. J. Pathol.* **163**, 2523–2530 (2003).
28. Couluris, M. *et al.* Treatment of idiopathic pulmonary fibrosis with losartan: a pilot project. *Lung* **190**, 523–527 (2012).
29. Kreuter, M. *et al.* Association of Angiotensin Modulators With the Course of Idiopathic Pulmonary Fibrosis. *Chest* **156**, 706–714 (2019).
30. Kim, M. D. *et al.* Losartan reduces cigarette smoke-induced airway inflammation and mucus hypersecretion. *ERJ Open Res.* **7**, 00394–02020 (2021).
31. Sikkema, L. *et al.* An integrated cell atlas of the lung in health and disease. *Nat. Med.* **29**, 1563–1577 (2023).
32. Moon, K. R. *et al.* Visualizing structure and transitions in high-dimensional biological data. *Nat. Biotechnol.* **37**, 1482–1492 (2019).
33. Wang, A. *et al.* Single-cell multiomic profiling of human lungs reveals cell-type-specific and age-dynamic control of SARS-CoV2 host genes. *eLife* **9**, (2020).

34. Rojas, M. *et al.* Aging and Lung Disease. Clinical Impact and Cellular and Molecular Pathways. *Ann. Am. Thorac. Soc.* **12**, S222-227 (2015).
35. Consortium, Gte. The GTEx Consortium atlas of genetic regulatory effects across human tissues. *Science* **369**, 1318–1330 (2020).
36. Chu, T., Wang, Z., Pe'er, D. & Danko, C. G. Cell type and gene expression deconvolution with BayesPrism enables Bayesian integrative analysis across bulk and single-cell RNA sequencing in oncology. *Nat. Cancer* **3**, 505–517 (2022).
37. Abadir, P. *et al.* Unlocking the protective potential of the angiotensin type 2 receptor (AT2R) in acute lung injury and age-related pulmonary dysfunction. *Biochem. Pharmacol.* **220**, 115978 (2024).
38. Adams, T. S. *et al.* Single-cell RNA-seq reveals ectopic and aberrant lung-resident cell populations in idiopathic pulmonary fibrosis. *Sci. Adv.* **6**, eaba1983 (2020).
39. Sauler, M. *et al.* Characterization of the COPD alveolar niche using single-cell RNA sequencing. *Nat. Commun.* **13**, 494 (2022).
40. Bonnardeaux, A. *et al.* Angiotensin II type 1 receptor gene polymorphisms in human essential hypertension. *Hypertension* **24**, 63–69 (1994).
41. Kobashi, G. *et al.* A1166C variant of angiotensin II type 1 receptor gene is associated with severe hypertension in pregnancy independently of T235 variant of angiotensinogen gene. *J. Hum. Genet.* **49**, 182–186 (2004).
42. Sethupathy, P. *et al.* Human microRNA-155 on chromosome 21 differentially interacts with its polymorphic target in the AGTR1 3' untranslated region: a mechanism for functional single-nucleotide polymorphisms related to phenotypes. *Am. J. Hum. Genet.* **81**, 405–413 (2007).
43. Wang, G., Sarkar, A., Carbonetto, P. & Stephens, M. A simple new approach to variable selection in regression, with application to genetic fine mapping. *J. R. Stat. Soc. Ser. B Stat. Methodol.* **82**, 1273–1300 (2020).
44. Hormozdiari, F. *et al.* Colocalization of GWAS and eQTL Signals Detects Target Genes. *Am. J. Hum. Genet.* **99**, 1245–1260 (2016).

45. Brown, A. A. *et al.* Predicting causal variants affecting expression by using whole-genome sequencing and RNA-seq from multiple human tissues. *Nat. Genet.* **49**, 1747–1751 (2017).

46. Wen, X., Pique-Regi, R. & Luca, F. Integrating molecular QTL data into genome-wide genetic association analysis: Probabilistic assessment of enrichment and colocalization. *PLoS Genet.* **13**, e1006646 (2017).

47. Denny, J. C. *et al.* Systematic comparison of phenome-wide association study of electronic medical record data and genome-wide association study data. *Nat. Biotechnol.* **31**, 1102–1110 (2013).

48. Wright, F. A. *et al.* Genome-wide association and linkage identify modifier loci of lung disease severity in cystic fibrosis at 11p13 and 20q13.2. *Nat. Genet.* **43**, 539–546 (2011).

49. Castranova, V., Rabovsky, J., Tucker, J. H. & Miles, P. R. The alveolar type II epithelial cell: a multifunctional pneumocyte. *Toxicol. Appl. Pharmacol.* **93**, 472–483 (1988).

50. Zeng, H. *et al.* LPS causes pericyte loss and microvascular dysfunction via disruption of Sirt3/angiopoietins/Tie-2 and HIF-2\alpha/Notch3 pathways. *Sci. Rep.* **6**, 20931 (2016).

51. Hung, C. F., Wilson, C. L. & Schnapp, L. M. Pericytes in the lung. *Adv. Exp. Med. Biol.* **1122**, 41–58 (2019).

52. Rosendahl, E. *et al.* Crafting a Patient-focused Phase 2b Trial (ASPIRE) to Evaluate Efficacy and Safety of Buloxibutid in Individuals With Idiopathic Pulmonary Fibrosis (IPF). in *B48. NEW TREATMENTS IN DIFFUSE PARENCHYMAL LUNG DISEASE* A3764–A3764 (American Thoracic Society, 2024). doi:10.1164/ajrccm-conference.2024.209.1_MeetingAbstracts.A3764.

53. Espitia-Corredor, J. A. *et al.* Angiotensin II Triggers NLRP3 Inflammasome Activation by a Ca2+ Signaling-Dependent Pathway in Rat Cardiac Fibroblast Ang-II by a Ca2+-Dependent Mechanism Triggers NLRP3 Inflammasome in CF. *Inflammation* **45**, 2498–2512 (2022).

54. Maté, I., Martínez de Toda, I., Arranz, L., Álvarez-Sala, J. L. & De la Fuente, M. Accelerated immunosenescence, oxidation and inflammation lead to a higher biological age in COPD patients. *Exp. Gerontol.* **154**, 111551 (2021).
55. König, I. R., Loley, C., Erdmann, J. & Ziegler, A. How to include chromosome X in your genome-wide association study. *Genet. Epidemiol.* **38**, 97–103 (2014).
56. Hayden, L. P. *et al.* X chromosome associations with chronic obstructive pulmonary disease and related phenotypes: an X chromosome-wide association study. *Respir. Res.* **24**, 38 (2023).
57. Stegle, O., Parts, L., Piipari, M., Winn, J. & Durbin, R. Using probabilistic estimation of expression residuals (PEER) to obtain increased power and interpretability of gene expression analyses. *Nat. Protoc.* **7**, 500–507 (2012).
58. McCarthy, D. J., Campbell, K. R., Lun, A. T. L. & Wills, Q. F. Scater: pre-processing, quality control, normalization and visualization of single-cell RNA-seq data in R. *Bioinformatics* **33**, 1179–1186 (2017).
59. Amezquita, R. A. *et al.* Orchestrating single-cell analysis with Bioconductor. *Nat. Methods* **17**, 137–145 (2020).
60. Waskom, M. seaborn: statistical data visualization. *J. Open Source Softw.* **6**, 3021 (2021).
61. Taylor-Weiner, A. *et al.* Scaling computational genomics to millions of individuals with GPUs. *Genome Biol.* **20**, 228 (2019).
62. Benjamin, K. J. M. *et al.* Analysis of the caudate nucleus transcriptome in individuals with schizophrenia highlights effects of antipsychotics and new risk genes. *Nat. Neurosci.* **25**, 1559–1568 (2022).
63. Benjamin, K. J. M. *et al.* Analysis of gene expression in the postmortem brain of neurotypical Black Americans reveals contributions of genetic ancestry. *Nat. Neurosci.* (2024) doi:10.1038/s41593-024-01636-0.
64. Yan, L. ggvenn: Draw Venn Diagram by 'ggplot2'. (2021).

65. Hao, Y. *et al.* Integrated analysis of multimodal single-cell data. *Cell* **184**, 3573-3587. (2021).

66. Kassambara, A. ggpubr: 'ggplot2' Based Publication Ready Plots. (2020).

67. Wickham, H. *Ggplot2 - Elegant Graphics for Data Analysis*. (Springer International Publishing, Cham, 2016). doi:10.1007/978-3-319-24277-4.

Acknowledgments

This research was supported by grants from the National Institutes of Health (NIH). A K99 Award (K99MD016964) from the National Institute on Minority Health and Health Disparities (NIMHD) supported KJMB, and awards R01HL154343 and R01HL160008 from the National Heart, Lung, and Blood Institute (NHLBI) supported ERN. The results shown here are also based upon data generated by the LungMAP Consortium [U01HL122642] and downloaded from (www.lungmap.net), on February 2nd, 2022. The LungMAP consortium and the LungMAP Data Coordinating Center (1U01HL122638) are funded by the NHLBI.

Author contributions

Conceptualization, KJMB and EN; Methodology, KJMB, MS, HP, and EN; Software, KJMB; Formal Analysis, KJMB; Data curation, KJMB, MS, and HP; Writing – original draft preparation, KJMB and EN; Writing – review and editing, KJMB, MS, and EN; Visualization, KJMB; Supervision, EN; Project administration, KJMB; Funding acquisition, KJMB.

Competing interest

The authors declare no competing interests.

Figure legends

Figure 1: Angiotensin II receptors 1 (*AGTR1*) and 2 (*AGTR2*) demonstrate compartment- and cell-type-specific expression in the human lung. A. Venn diagram showing rare occurrences of *AGTR1* and *AGTR2* co-expression (n=107 individuals). **B.** Dot plot showing the percentage and average expression of *AGTR1*- and *AGTR2*-positive cells across lung compartments (n=107). **C.** Heatmap showing significant enrichment (two-sided, Fisher's exact test) of *AGTR1*- and *AGTR2*-positive cells across lung compartments (n=107). The color intensity of enrichment heatmaps represents log2 of odds ratio (OR) with red indicating enrichment and blue indicating depletion. Significantly enrichment compartments are annotated with -log10(false discovery rate). **D.** Dotplot showing the percentage and average expression of *AGTR1*- and *AGTR2*-positive cells across lung cell types (n=107).

Figure 2: *AGTR1* is a global marker for pericytes. A. Scatter plot showing pericyte subclusters using PHATE dimensional reduction[32]. Subclusters are highlighted using K-means clustering. **B.** Scatter plot showing normalized expression of *AGTR1* across pericyte subclusters. **C.** Box plot showing no significant differences of AGTR1 normalized expression across pericyte subclusters after averaging across individuals (n=107 across clusters). Box plots show the median and first and third quartiles, and whiskers extend to 1.5x the interquartile range.

Figure 3: Angiotensin receptors, *AGTR1* and *AGTR2*, show distinct developmental trajectories across the lung location. A. Dotplot of average expression and percent expression from total cells separated by age. **B.** Line graph showing average number of cells (left) and log normalized expression (right) as a function of age. **C.** Line graph showing average number of cells (top) and log normalized expression (bottom) as a function of age separated by LungMAP annotated lung location. Three donors per age group. The standard error is annotated with error bars for all line graphs. Mean averaged across the three unique individuals are also annotated within the error bars, shown as standard error, of the line graphs. Solid line, *AGTR1*. Dash line, *AGTR2*.

Figure 4: Replication of the angiotensin receptors' distinct developmental trajectories in bulk RNA-sequence analysis. A. Line graph of log2 normalized expression in bulk LungMAP lung tissue (n=3 per age group; error bars, standard error). Solid line, *AGTR1*. Dash line, *AGTR2*. **B.** Scatterplots of angiotensin receptors showing normalized expression as a function of age in adults (age > 20) from GTEx bulk lung tissue (n=578). **C.** Scatterplot showing the proportion of AT2 (alveolar epithelial type 2) and alveolar macrophage cell types from deconvoluted GTEx bulk tissue decreasing as a function of age (left), while normalized *AGTR2* expression increased with AT2 proportion (right). **D.** Scatterplot showing the cell type proportions of cell types enriched for *AGTR1* enriched cells (i.e., pericytes, adventitial fibroblasts, alveolar fibroblasts, peribronchial fibroblasts, and smooth muscle) from deconvoluted GTEx bulk tissue as a function of age. **E.** Scatterplots of normalized angiotensin receptors expression as a function of pericytes (top), adventitial fibroblasts (middle), and alveolar fibroblasts (bottom) cell type proportions. Blue line fitted trend (two-sided, Pearson's correlation). The 95% confidence interval is shaded in gray.

Figure 5: Fibroblasts and alveolar epithelial type 2 (AT2 subpopulation) are significantly upregulated in individuals with COPD for *AGTR1* and *AGTR2*,

respectively. A. Venn diagram showing limited co-occurrence of *AGTR1* and *AGTR2* expression in the same cell (control [n=28], COPD [n=18], or IPF [n=32][38]). **B.** Dotplot of average and percent expression of angiotensin receptors from total cells separated by diagnosis (control [n=28], COPD [n=18], or IPF [n=32][38]). Box plot comparing IPF (n=32), COPD (n=18), and control donors (n=28) normalized expression for cell types enriched for **C.** *AGTR1*-positive cells and **D.** *AGTR2*-positive cells. **E.** Dotplot of average and percent expression of angiotensin receptors showing enrichment of *AGTR2* expression for AT2 subpopulation ($AT2_B$; COPD [n=17] and age-matched control donors [n=15][39]). **F.** Box plot of normalized expression for AT2 subpopulation ($AT2_B$) comparing COPD (n=17) and age-matched control donors (n=15). **G.** Replication of *AGTR2* upregulation for COPD for AT2 subpopulation within IPF/COPD dataset (control [n=28], COPD [n=18], or IPF [n=32][38]). Top: Dimensional reduction using PHATE[32] of AT2 in IPF/COPD dataset showing two subclusters (0 and 1). Bottom: Heatmap showing limited expression of *AGTR2* specific to PHATE subcluster 1. **H.** Box plot of normalized expression for PHATE AT2 subclusters showing increased expression of *AGTR2* for COPD compared with control donors. Box plots are annotated with a two-sided, t-test and show the median and first and third quartiles, and whiskers extend to 1.5x the interquartile range.

Supplementary information

Figures

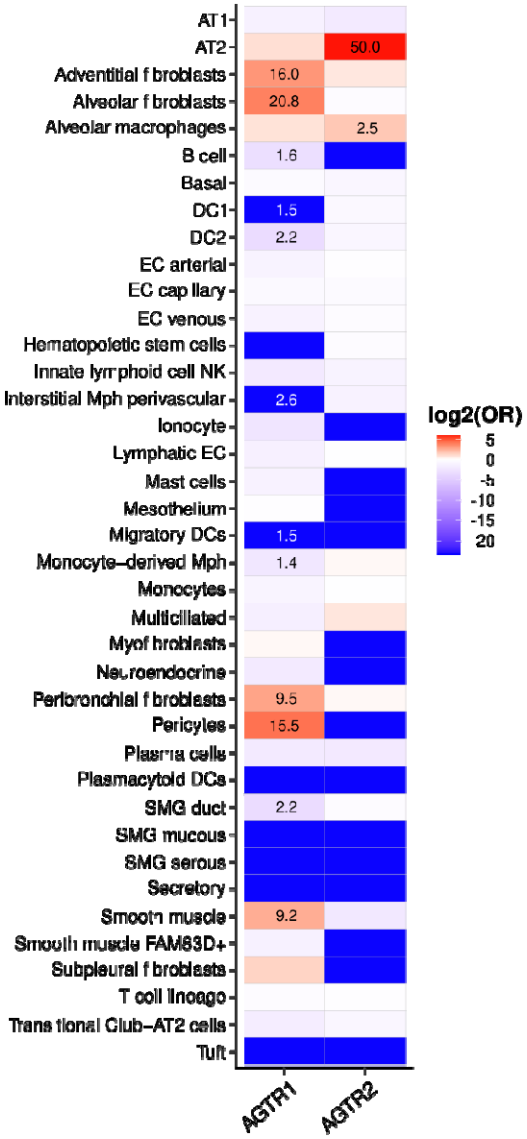

Figure S1: Angiotensin II receptors 1 *(AGTR1)* and 2 *(AGTR2)* show cell-type-specific enrichment in the human lung. Heatmap showing significant enrichment (two-sided, Fisher's exact test) of *AGTR1*- and *AGTR2*-positive cells across lung cell types (n=107). The color intensity of enrichment heatmaps represents log2 of odds ratio (OR) with red indicating enrichment and blue indicating depletion. Significantly enrichment compartments cell types are annotated with -log10(false discovery rate).

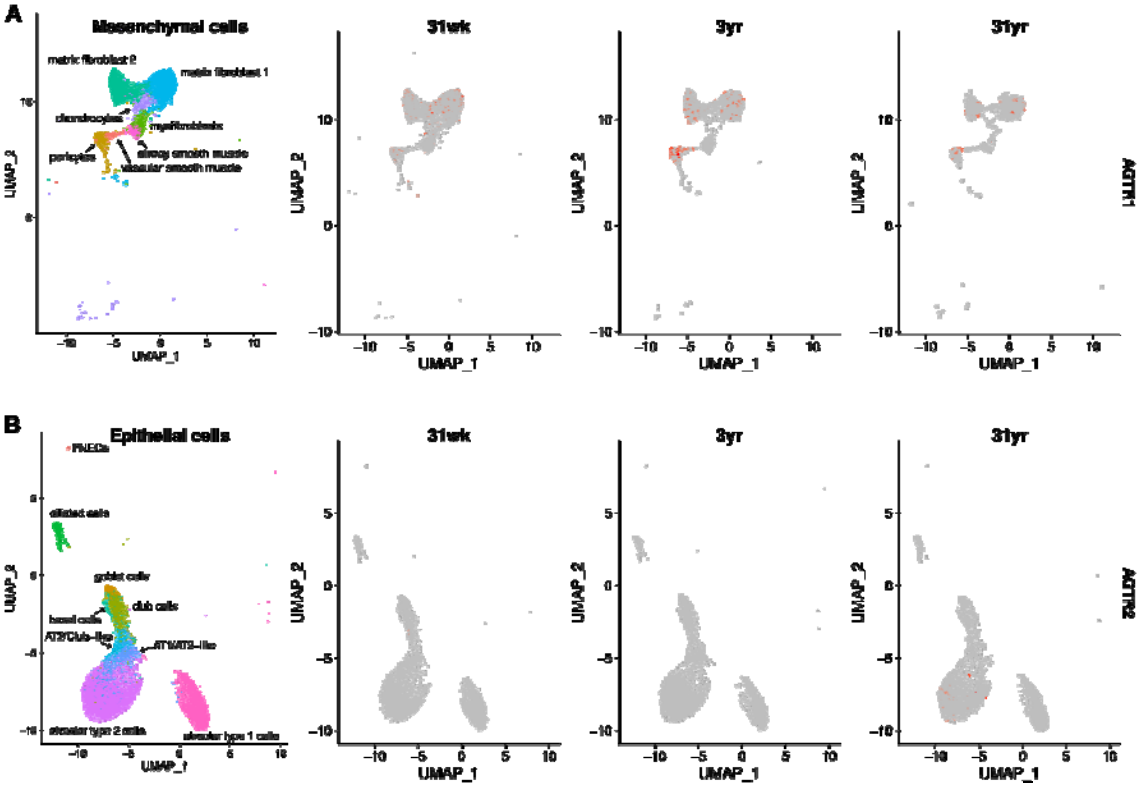

Figure S2: The stable *AGTR1* expression was associated with a decrease in mesenchymal cells as a function of age, while *AGTR2* expression in AT2 epithelial cells increases with age. UMAP of **A.** mesenchymal and **B.** epithelial cells subset by age. Mesenchymal cells decrease with age, while epithelial cells are stable.

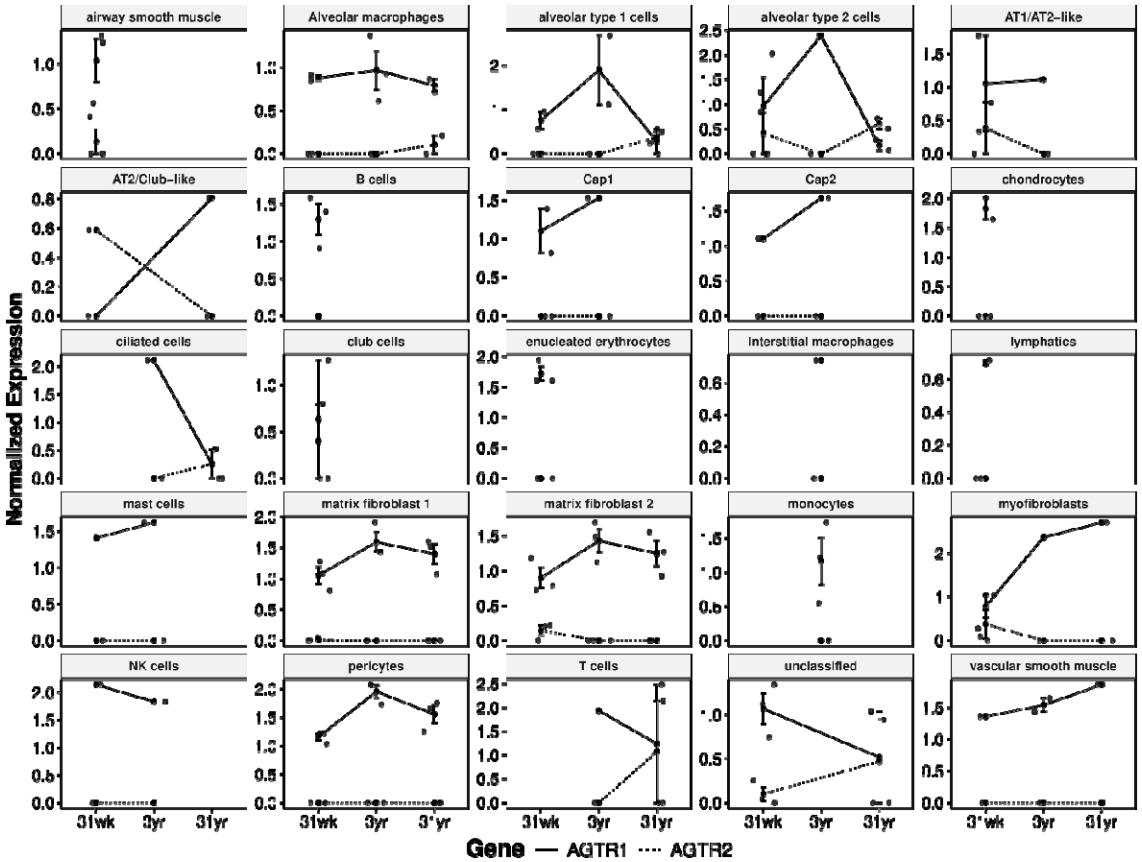

Figure S3: Angiotensin receptors show distinct expression developmental trajectories across cell types. Line graph showing log2 normalized expression as a function of age separated by LungMAP annotated lung cell types. Three donors per age group. Error bars show standard error. Solid line, *AGTR1*. Dash line, *AGTR2*.

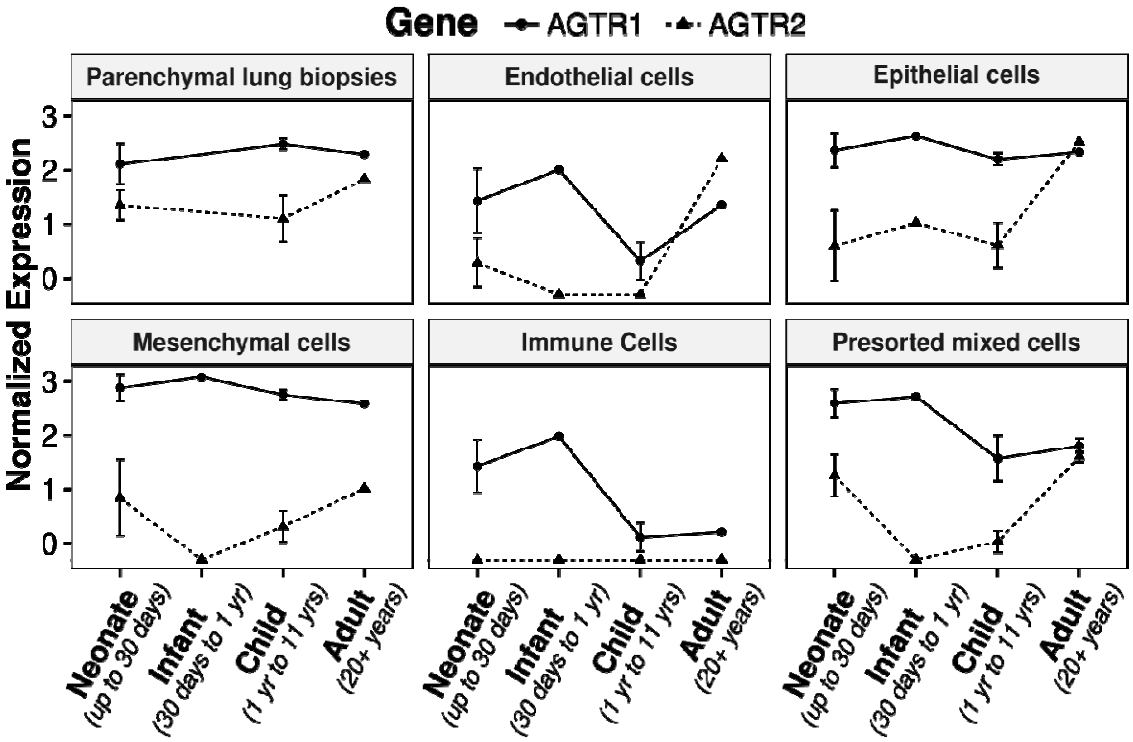

Figure S4: Angiotensin II receptor expression varies with age across cell type groups (endothelial, epithelial, mesenchymal [stromal], and immune cells), bulk lung, and mixed cells. Line graph of log2 normalized expression in bulk LungMAP lung tissue (n=3 per age group; error bars show standard error). Solid line, *AGTR1*. Dash line, *AGTR2*.

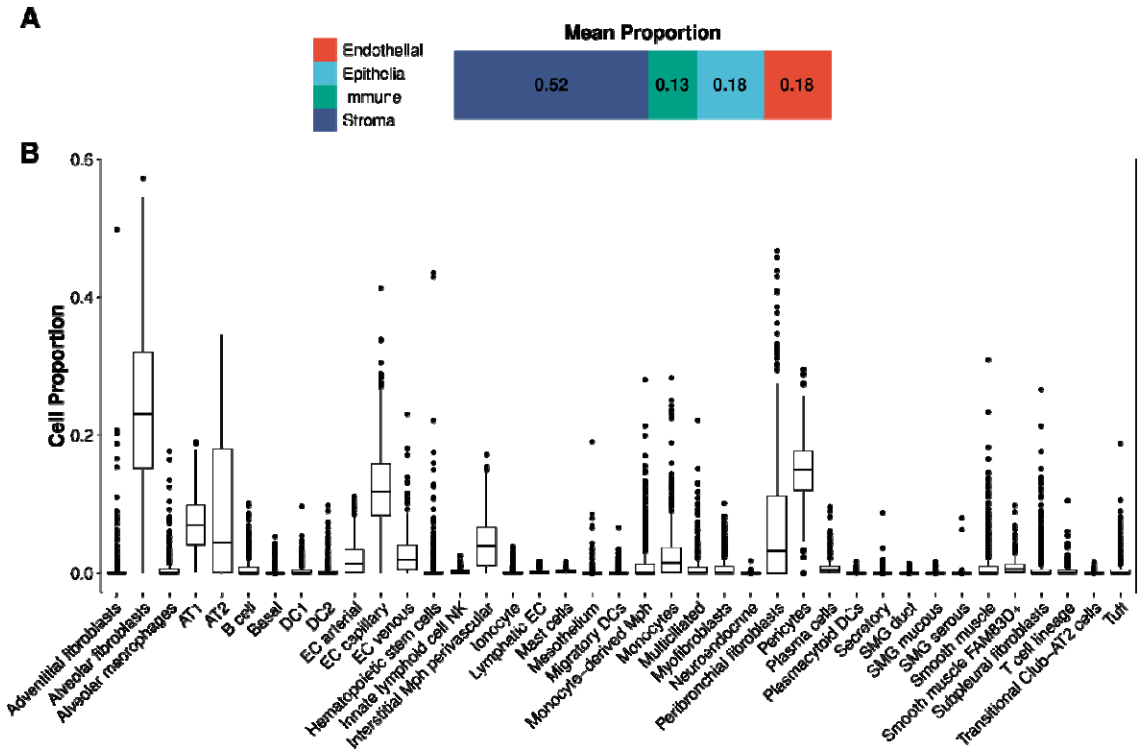

Figure S5: Cell type deconvolution of the GTEx lung using Human Lung Cell Atlas version 2. Barplot showing mean cell proportions of **A.** compartment from cell type deconvolution of the GTEx lung. **B.** Box plots showing cell proportion from annotated cell type deconvolution of the GTEx lung (n=578). Box plots show the median and first and third quartiles, whiskers extend to 1.5× the interquartile range, and outlier samples are plotted as black circles.

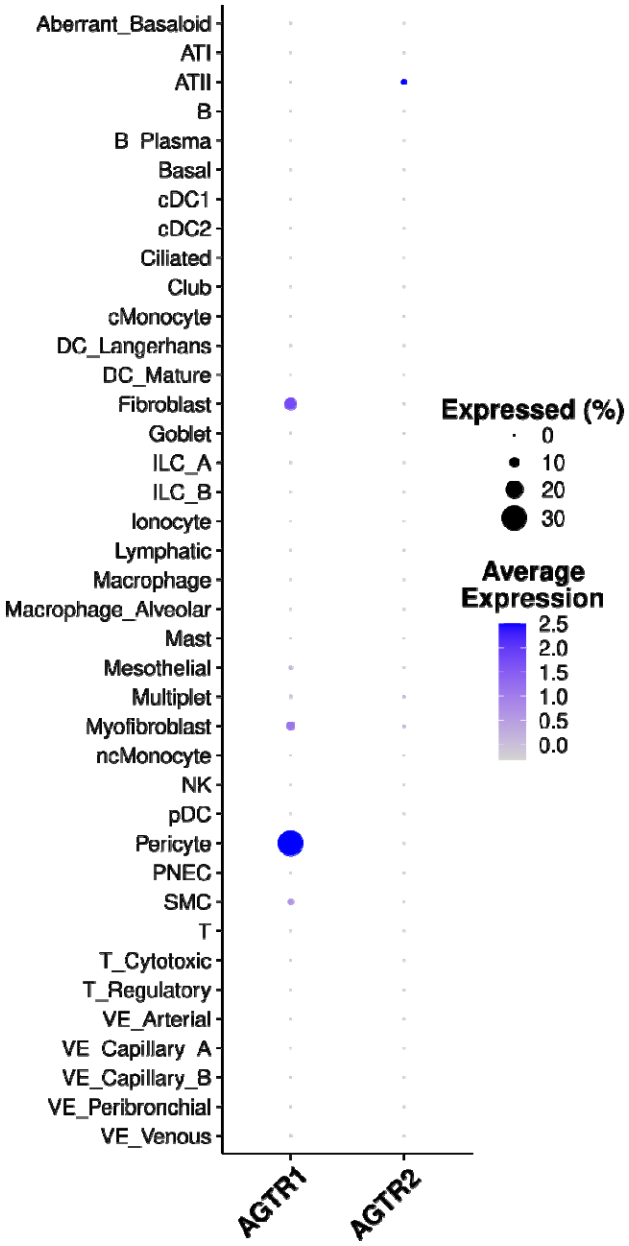

Figure S6: Replication of angiotensin receptors distinct localization in IPF/COPD dataset. Dot plot showing cell type-specific expression of *AGTR1* (pericyte, fibroblast, myofibroblast, and smooth muscle cells [SMC]) and *AGTR2* (AT2).

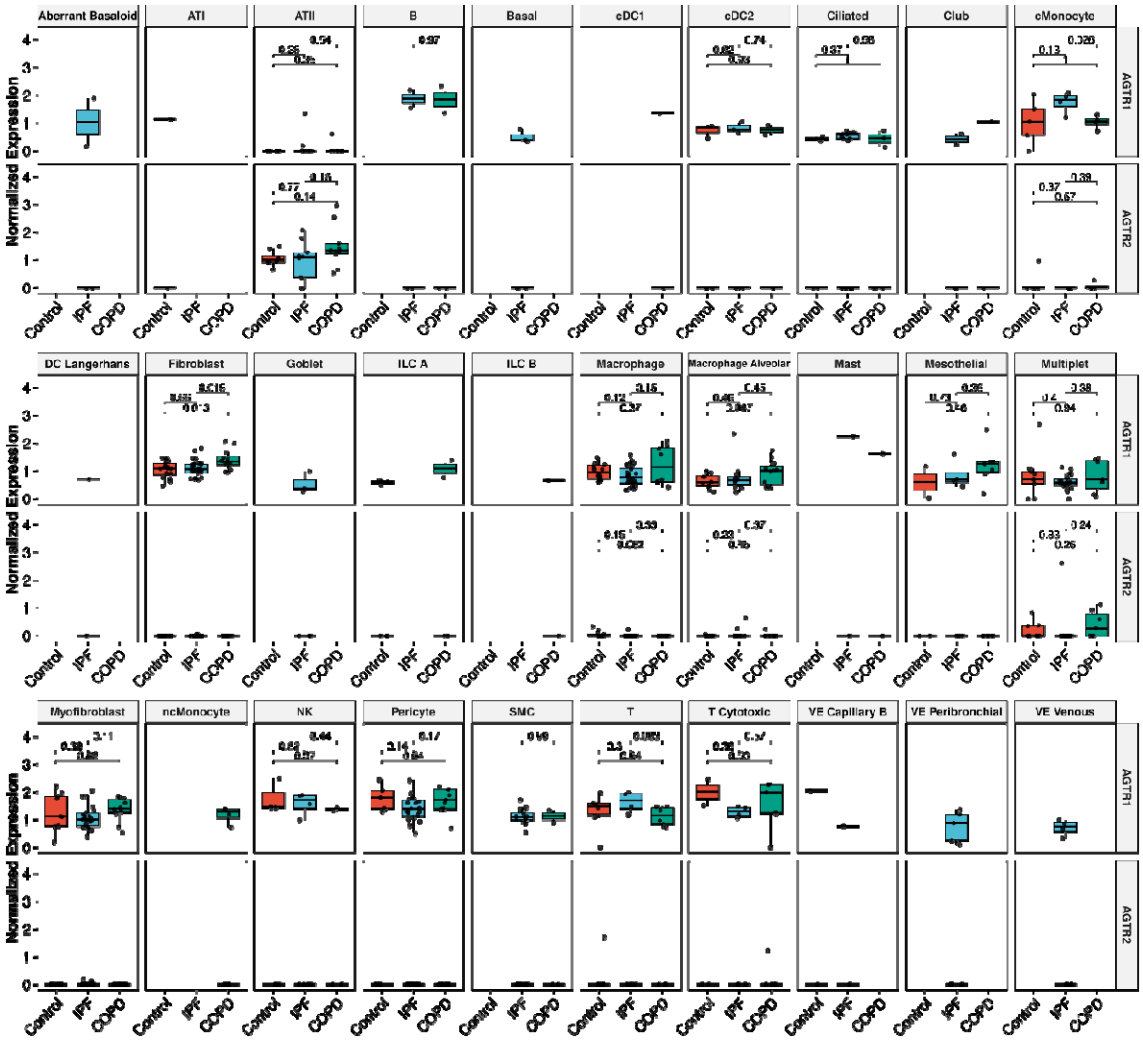

Figure S7: Angiotensin receptor expression is not significantly dysregulated in IPF. Box plots showing normalized expression by diagnosis across lung cell types after filtering for AGTR1- and AGTR2-positive cells (control [n=28], COPD [n=18], or IPF [n=32][38]). P-values from one-sided T-test are annotated for cell types with enough individuals after filtering. Box plots show the median and first and third quartiles, whiskers extend to 1.5× the interquartile range, and outlier samples are plotted as black circles.

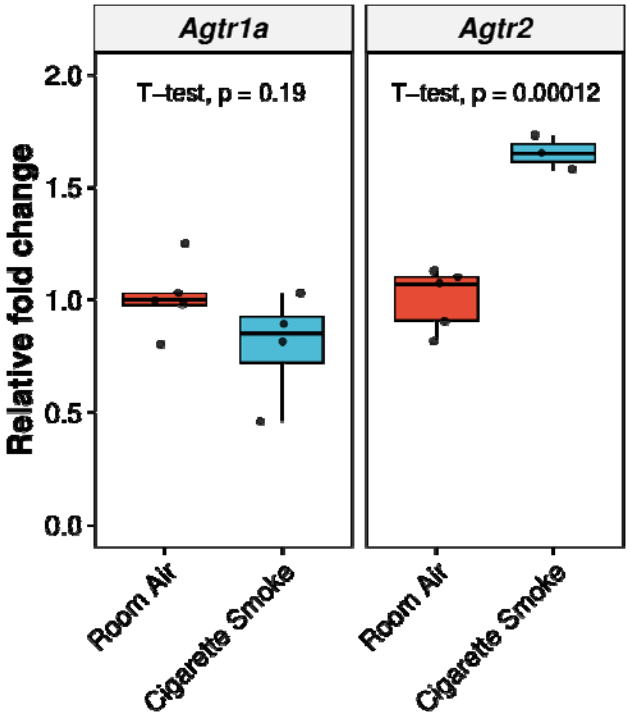

Figure S8: Angiotensin receptor 2 (*Agtr2*) expression is increased in the cigarette smoke-exposed mouse lung. Box plot of real-time PCR quantitation of *Agtr1a* (n=4) and *Agtr2* (n=3) expression in cigarette smoke-exposed mice compared with room air controls (n=5). Receptor expression was normalized to *Gapdh*. Box plots show the median and first and third quartiles, whiskers extend to 1.5× the interquartile range, and outlier samples are plotted as black circles.

Supplementary Tables

Table S1: Summary of significant eQTL (permutation q-value < 0.05) for *AGTR1* and *AGTR2* from re-processed GTEx lung data (n=578).

Table S2: Summary of conditional eQTL for *AGTR1* and *AGTR2* from re-processed GTEx lung data (n=578).

Table S3: Summary of SuSIE fine-mapping results for angiotensin receptors (*AGTR1* and *AGTR2*) using GTEx lung data (n=578).

Table S4: Subset of CaVEMaN fine-mapped results from GTEx lung (n=578) for *AGTR1* and *AGTR2*.

Table S5: Subset of CAVIAR fine-mapped results from GTEx lung (n=578) for *AGTR1* and *AGTR2*.

Table S6: Subset of DAP-G fine-mapped results from GTEx lung (n=578) for *AGTR1* and *AGTR2*.

Table S7: Subset of DAP-G CS95 fine-mapped results from GTEx lung (n=578) for *AGTR1* and *AGTR2*.

Table S8: Summary of phenotypes significantly associated (p-value < 0.05) with *AGTR2* fine-mapped SNP, rs1403543, in the PheWAS catalog.